Because of the small number of species and the uncertainty in absolute dating, there is uncertainty in our estimate of extinction rate. But because the relation between estimated extinction rate and estimated preservation rate is linear, the value of q would have to be more than an order of magnitude lower than our estimate in order to affect our conclusions substantially. Taxonomic rates this low are incompatible with rates estimated for Cenozoic mammals (*14*, *24*, *25*) and for even the most slowly evolving groups of animals (*25*).
29. Because of the difference between Cenozoic and Cretaceous preservation rates, we do not recommend using Cenozoic occurrences to place confidence limits (*15*) on stratigraphic ranges for mammal taxa that may extend into the Cretaceous [see also (*10*)]. Moreover, confidence limits are more difficult to estimate for higher taxa than for single species, because the probability of group preservation per unit time is potentially greatly affected by changes in diversity [R. Bleiweiss, *Geology* **26**, 323 (1998); C. R. Marshall and R. Bleiweiss, *ibid.* **27**, 95 (1999)].
30. M. Messer *et al.*, *J. Mammal. Evol.* **5**, 95 (1998).
31. It is also likely that preservation rate fluctuates over time, because sea level and other factors change. Modeling of time-heterogeneous preservation (*14*, *24*), however, shows that fluctuating preservation rate is not likely to distort substantially either the overall probability of species preservation or our estimates of preservation rate.
32. M. S. Springer *et al.*, *Nature* **388**, 61 (1997); M. J. Stanhope *et al.*, *Mol. Phylogenet. Evol.* **9**, 501 (1998); M. J. Stanhope *et al.*, *Proc. Natl. Acad. Sci. U.S.A.* **95**, 9967 (1998).
33. P. D. Gingerich, *Mol. Biol. Evol.* **3**, 205 (1986).
34. R. J. Britten, *Science* **231**, 1393 (1986).
35. J. H. Gillespie, *Proc. Natl. Acad. Sci. U.S.A.* **81**, 8009 (1984); *Genetics* **113**, 1077 (1986); *Mol. Biol. Evol.* **3**, 138 (1986); M. M. Miyamoto and W. M. Fitch, *ibid.* **12**, 503 (1995).
36. M. Goodman, *Prog. Biophys. Mol. Biol.* **37**, 105 (1981).
37. D. M. Raup, in *Rates of Evolution*, K. S. W. Campbell and M. F. Day, Eds. (Allen & Unwin, London, 1986), pp. 1–14.
38. If molecular rates are faster during evolutionary radiations, this may reflect two end-member mechanisms that have been suggested previously: (i) Adaptive change within species is faster during the rapid occupation of new adaptive zones (*41*), and many molecular substitutions are selective rather than neutral (*35*, *36*); or (ii) a punctuational model applies to molecular evolution, with change concentrated at lineage splitting; thus, rapid speciation during evolutionary radiation (*41*) causes faster molecular rates (*37*). These mechanisms are testable with data from extant groups for which fossil diversity, genealogical relationships, and fossil divergence times are reliably known: Each pair of living species is separated by a divergence time, a number of cladogenetic events (patristic distance), a morphological distance, and a molecular distance. If morphological divergence provides a measure of adaptive change, the first hypothesis implies a positive partial correlation between molecular and morphological distance, with divergence time and patristic distance held statistically constant. The second hypothesis implies a positive partial correlation between molecular and patristic distance, with divergence time and morphological distance held constant.
39. M. C. McKenna and S. K. Bell, *Classification of Mammals Above the Species Level* (Columbia Univ. Press, New York, 1997).
40. Occurrence data are from a compilation of faunal lists and synonymies, extensively supplemented with observations by J.P.H. This database is heavily influenced by the rich fossil record of North America, but also includes the known faunas of South America, Europe, Asia (Mongolia, India, and western Asia), and Madagascar. Biostratigraphic correlation for species outside North America was based largely on information in the references consulted for faunal lists. For North American species, these sources were supplemented by the following: J. A. Lillegraven, *Contrib. Sci. Los Angeles Co. Mus.* **232**, 1 (1972); _____ and L. M. Ostresh Jr., *Geol. Soc. Am. Spec. Pap.* **243**, 1 (1990); M. B. Goodwin and A. L. Deino, *Can. J. Earth Sci.* **26**, 1384 (1989); R. R. Rogers, C. C. Swisher III, J. R. Horner, *ibid.* **30**, 1066 (1993); C. C. Swisher III, L. Dingus, R. F. Butler, *ibid.*, p. 1981; F. M. Gradstein *et al.*, in *Geochronology, Time Scales and Global Stratigraphic Correlation*, W. A. Berggren, D. V. Kent, M.-P. Aubry, J. Hardenbol, Eds. [Society for Sedimentary Geology (SEPM), Tulsa, OK], pp. 95–126. To determine whether a species is known from a single horizon, it is generally necessary to have only a relative biochronology. We did not base our relative chronology solely on faunal associations of mammals, but also used local and regional stratigraphic relations, radiometric dates, and correlations with marine sequences based largely on regional strandline stratigraphy, as derived from sources cited above. North American localities were arranged into 14 resolvable stratigraphic intervals, and the localities of other continents were resolved to between 1 and 3 intervals, depending on the region. We treated each of these intervals operationally as a horizon. This approach is conservative insofar as it lumps distinct horizons into one unit, overestimating the proportion of species confined to single horizons and thus underestimating preservation rate. Our approach is also conservative insofar as we generally considered species with uncertain stratigraphic ranges as single-horizon taxa. To estimate average stratigraphic ranges of North American species, for which the biochronology is best understood, we assigned absolute ages to the 14 stratigraphic intervals, mainly using correlations with ammonite zones and radiometric dates. See supplemental data at www.sciencemag.org/feature/data/985988.shl.
41. S. M. Stanley, *Macroevolution* (Freeman, San Francisco, 1979).
42. W. B. Harland *et al.*, *A Geologic Time Scale 1989* (Cambridge Univ. Press, Cambridge, 1990).
43. E. Gheerbrant, J. Sudre, H. Cappetta, *Nature* **383**, 68 (1996).
44. R. C. Fox and G. P. Youzwyshyn, *J. Vertebr. Paleontol.* **14**, 382 (1994).
45. We thank J. Alroy, R. J. Asher, J. Flynn, D. Jablonski, C. R. Marshall, R. R. Rogers, P. J. Wagner, and J. R. Wible for discussion, and R. H. De Simone, D. Jablonski, C. R. Marshall, D. M. Raup, and two anonymous referees for reviews. This research was supported by NSF (grant EAR-9506568) and NASA (grant NAGW-1693).

20 October 1998; accepted 27 January 1999

The Density of Hydrous Magmatic Liquids

Frederick A. Ochs III and Rebecca A. Lange

Density measurements on several hydrous (≤19 mole percent of H_2O) silicate melts demonstrate that dissolved water has a partial molar volume ($\bar{V}_{H_2O}$) that is independent of the silicate melt composition, the total water concentration, and the speciation of water. The derived value for $\bar{V}_{H_2O}$ is 22.9 ± 0.6 cubic centimeters per mole at 1000°C and 1 bar of pressure, whereas the partial molar thermal expansivity ($\partial\bar{V}_{H_2O}/\partial T$) and compressibility ($\partial\bar{V}_{H_2O}/\partial P$) are 9.5 ± 0.8 × 10^{-3} cubic centimeters per mole per kelvin and −3.2 ± 0.6 × 10^{-4} cubic centimeters per mole per bar, respectively. The effect of 1 weight percent dissolved H_2O on the density of a basaltic melt is equivalent to increasing the temperature of the melt by ~400°C or decreasing the pressure of the melt by ~500 megapascals. These measurements are used to illustrate the viability of plagioclase sinking in iron-rich basaltic liquids and the dominance of compositional convection in hydrous magma chambers.

The density of a silicate melt affects a wide range of magmatic processes, including melt segregation and transport, melt recharge and mixing in chambers, the viability of convection and crystal settling, and the mechanics of eruption. Water is an important component to include in models of melt density, as it can range up to 8 weight % in magmatic liquids (*1*), which translates to ~25 mol % because of the low molecular weight of H_2O as compared to the average molecular weight of magmatic liquids. Before this study, the only direct density measurements available for hydrous silicate melts were performed on molten albite ($NaAlSi_3O_8$) (*2*, *3*). The large partial molar volume of the H_2O component (total water dissolved as molecular H_2O and as hydroxyl ions), $\bar{V}_{H_2O}$, in albitic melt (*3*) results in a low density for the H_2O component (0.78 g/cm^3) as compared to the density range of magmatic liquids (2.3 to 2.8 g/cm^3). This leads to a dramatic effect of dissolved water on melt density. For example, if the value for $\bar{V}_{H_2O}(T, P)$ (T, temperature; P, pressure) derived from albitic liquid is applied to the Bishop Tuff rhyolite, then the effect on melt density of adding 1 weight % H_2O (at 750°C and 300 MPa) is equivalent to increasing the temperature by 620°C or decreasing the pressure by 260 MPa (the results are different for a basalt, which is less compressible and more thermally expansive than a rhyolite).

The outstanding question is whether the values for $\bar{V}_{H_2O}(T, P)$ derived for molten albite (*3*) can be applied to all igneous liquids or whether there is a compositional dependence to $\bar{V}_{H_2O}(T, P)$. An indirect method for determining $\bar{V}_{H_2O}$, which has been applied to a variety of silicate melts, is based on fitting a thermodynamic model to the solubility of water. The pressure dependence of the solu-

Department of Geological Sciences, University of Michigan, Ann Arbor, MI 48109–1063, USA.

bility of water is a function of $\bar{V}_{H_2O}$; unfortunately, it is also a function of other parameters that must be estimated, the least certain of which is the activity-composition relation for the H_2O component. Derived values of $\bar{V}_{H_2O}$ can vary by a factor of 2, depending on the form of the activity-composition relation that is assumed. Further, the value of $\bar{V}_{H_2O}$ estimated in this manner is an average over the pressure range of the solubility experiments. Because the H_2O component is so compressible in silicate melts (*2, 3*), averaging $\bar{V}_{H_2O}$ over several hundred megapascals leads to an imprecise value.

The uncertainty with the activity-composition relation for H_2O can be resolved, in part, if the solubility of molecular water (instead of total water) is used because there is evidence that it follows Henry's Law (*4*). However, the solubility of molecular water is not well known because of the difficulty in quenching the ratio of molecular water to hydroxyl groups in high-temperature melts into the glass at room temperature. Despite these problems, the solubility method has led to a wide range of published values for $\bar{V}_{H_2O}$ and $\bar{V}_{H_2O_{molecular}}$ (the partial molar volume of dissolved molecular water) that vary with melt composition. For example, derived values of $\bar{V}_{H_2O_{molecular}}$ are 22 and 0 cm^3/mol in albite and rhyolite melt, respectively (*4*). These results have led to the question of whether there is a compositional dependence to $\bar{V}_{H_2O}(T, P)$, which our study directly tests by measuring the density of hydrous rhyolitic melts and comparing the results to those for albite (*2, 3*). Because rhyolite and albite are fully polymerized liquids [the ratio of nonbridging oxygen to tetrahedrally coordinated cation, NBO/T, is ~0 (*5*)], a second, depolymerized melt (a melt with NBO/T = 1.9; hereafter referred to as KCS) was also used in this study. These two melt compositions (Table 1) (*6, 7*) were chosen to test whether the degree of polymerization or the presence of Na_2O and Al_2O_3 [two components shown to significantly affect water solubility in natural silicate liquids (*8*)] has any effect on derived values of $\bar{V}_{H_2O}(T, P)$. We also determined whether $\bar{V}_{H_2O}(T, P)$ depends on the speciation of water between molecular water and hydroxyl groups.

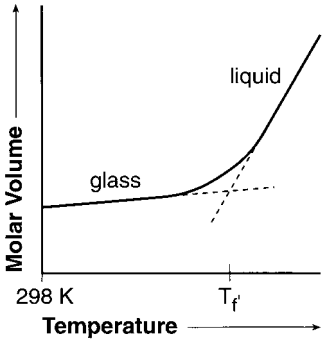

Fig. 1. Schematic diagram of the molar volume of a sample (solid line) as a function of temperature during cooling from a liquid to a glass. The limiting fictive temperature ($T_{f'}$) is defined as the intersection of the extrapolated equilibrium liquid and the glass volume curves (dashed lines). The deviation from the dashed lines near $T_{f'}$ is caused by kinetic effects. For a more detailed discussion, see (*9, 13*).

Because hydrous silicate melts devolatilize at room pressure, our study exploits the thermodynamic and kinetic properties of the liquid-glass transition to measure the density of a hydrous silicate liquid at 1 bar (*3*). When a liquid is rapidly cooled through the glass transition interval, temperature-induced structural rearrangements become kinetically impeded, and eventually the structure of the liquid is "frozen" into the glass. The structure preserved in the glass is the equilibrium structure of the liquid at T_f', which is defined as the temperature at which an extrapolated first-order property of the glass and the liquid are the same (*9*). Therefore, the molar volume of the glass is equal to that of the liquid at T_f' (Fig. 1). The volume of a liquid at T_f' ($V^{liq}_{T_f'}$) can thus be obtained by quenching a melt to a glass and measuring (i) the 1-bar, 298 K density of the glass (*10*), (ii) the coefficient of thermal expansion for the glass (α^{glass}), and (iii) the value of T_f'. The relation is shown in the following equation

$$V^{liq}_{T_{f'}} = V^{glass}_{T_{f'}} = V^{glass}_{298\ K} \exp \int_{298\ K}^{T_{f'}} \alpha^{glass} dT \quad (1)$$

Hydrous glass samples were synthesized in a piston-cylinder apparatus (Table 2) and quenched isobarically. Only samples that were free of bubbles, crystallites, and cracks were used. Water content was measured in the rhyolitic glasses by Fourier transform infrared (FTIR) spectroscopy, whereas manometry (vacuum fusion and H_2O extraction) and FTIR spectroscopy were used to measure the water concentration in the KCS glasses (*11*). In all cases, water was evenly distributed in the sample glasses. The room temperature density ($\rho^{glass}_{298\ K}$) of each sample was measured by weighing its mass in air and in toluene with a microbalance. Because the hydrous glasses were synthesized at high pressure, a correction was made to adjust their density to 1-bar values (*12*). The α^{glass} and T_f' of each sample were measured with a Perkin-Elmer TMA-7 dilatometer using a scan rate of 10 K/min (*3, 13*). FTIR spectra taken before and after the thermal expansion measurements demonstrate that no H_2O was lost during the dilatometry runs at temperatures <50°C above T_f'. The measured values for $\rho^{glass}_{298\ K}$, α^{glass}, and T_f' for each hydrous glass are listed in Table 2, as well as the calculated liquid volumes at T_f' ($V^{liq}_{T_f'}$) from Eq. 1.

To derive a value of $\bar{V}_{H_2O}(T, P)$ that can be applied to magmatic silicate melts, we fitted the hydrous density data for KCS, rhyolite (Table 2), and albite (*2, 3*) to the following model equation

$$V(T,P,X) = X_i[\bar{V}_{i,T_{ref}} + \partial\bar{V}_i/\partial T(T - T_{ref}) + \partial\bar{V}_i/\partial P(P - P_{ref})] \quad (2)$$

where $\bar{V}_i$, $\partial\bar{V}_i/\partial T$, and $\partial\bar{V}_i/\partial P$ are the partial molar volume, thermal expansivity, and compressibility of each oxide component, respec-

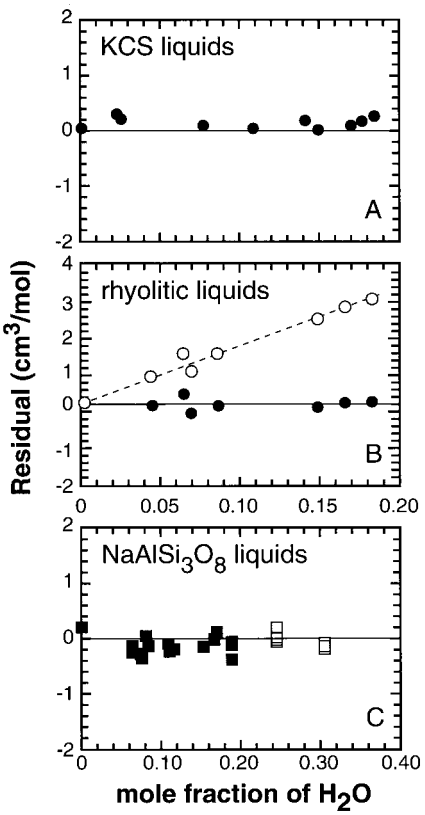

Fig. 2. A plot of residuals (measured minus calculated volumes) for the hydrous experimental liquids as a function of dissolved water content. (**A**) KCS liquids. (**B**) Rhyolite liquids (solid circles) and rhyolite liquids assuming $\bar{V}_{H_2O}$ = 0 cm^3/mol (open circles). (**C**) $NaAlSi_3O_8$ liquids. Open squares are data from (*2*) and solid squares are data from (*3*). The data from (*2*) extend up to 1201 K and 0.84 GPa. The quality of the fit for all three liquids demonstrates that the measurements reported in this study are consistent with (*2*), despite the fact that different techniques were employed.

Table 1. Starting glass compositions from (*6, 7*) and normalized to mole percent.

Oxide	KCS	Rhyolite*
SiO_2	59.51	83.58
Al_2O_3	–	7.98
MgO	–	0.13
CaO	30.51	0.70
Na_2O	–	4.26
K_2O	9.97	3.35

*FeO^T was lost to Pt capsule during synthesis.

tively; X_i is the mole fraction of each oxide component; and T_{ref} and P_{ref} are the reference temperature and pressure (1000°C and 1 bar). Because values for $\bar{V}_i$, $\partial\bar{V}_i/\partial T$, and $\partial\bar{V}_i/\partial P$ for the anhydrous components are well constrained from previously published 1-bar density (*6, 13, 14*) and sound speed (*15*) measurements (with substantially smaller errors than those associated with the hydrous liquids), their contributions were calculated with the model of (*16*) and were subtracted from the measured volumes of the hydrous liquids. The resultant volume data were fitted to a simplified form of Eq. 2, in which only the volumetric properties of the H_2O component were derived. This approach to the regression effectively places all of the experimental error on the values for the H_2O component. At 1000°C and 1 bar (±1σ), they are $\bar{V}_{H_2O}$ = 22.89 (±0.55) cm³/mol, $\partial\bar{V}_{H_2O}/\partial T$ = 9.46 (±0.83) × 10^{-3} cm³/mol-K, and $\partial\bar{V}_{H_2O}/\partial P$ = −3.15 (±0.61) × 10^{-4} cm³/mol-bar. These regressed values can be used with the model of (*16*) to calculate the density of any natural silicate melt.

The residuals (measured minus calculated volumes) for all three hydrous liquids (KCS, rhyolite, and albite) are plotted versus dissolved water content in Fig. 2. In 70 out of 75 cases, the residuals are within the ±1.1% uncertainty of the measurements (*17*), and the average residual is 0.6%, which demonstrates that the volumes of all three hydrous liquid compositions are fitted equally well with the same value of $\bar{V}_{H_2O}(T, P)$. The residuals are plotted in Fig. 2B for the case in which $\bar{V}_{H_2O}$ = 0; our measurements show that $\bar{V}_{H_2O}$ cannot be zero in rhyolitic melts. Moreover, because there is no increase in the residuals with increasing H_2O concentration, our results indicate that $\bar{V}_{H_2O}(T, P)$ is independent of total water concentration and water speciation; as the total water concentration increases, so does the concentration of molecular water relative to hydroxyl ions in our experimental liquids at T_f' (Table 2), and yet the value for $\bar{V}_{H_2O}(T, P)$ remains constant. In summary, our measurements demonstrate no variation in $\bar{V}_{H_2O}(T, P)$ related to melt composition, total water content, or water speciation.

Our fitted values for $\partial\bar{V}_{H_2O}/\partial T$ and $\partial\bar{V}_{H_2O}/\partial P$ in silicate liquids are more than three times larger than their corresponding values in silicate glasses (*3, 18*). This difference reflects the abrupt jump observed for second-order thermodynamic properties at the glass-liquid transition. Similarly, our range of values for $\bar{V}_{H_2O}(T, P)$ in silicate melts under magmatic crustal conditions (between 750° and 1250°C and 0 to 1 GPa) is substantially larger (17 to 25 cm³/mol) than the value for $\bar{V}_{H_2O}$ of ~12 cm³/mol derived from compressed hydrous glasses at room temperature (*18*), again reflecting the difference between glass and liquid properties. However, the value for $\bar{V}_{H_2O}$ based on a linear regression of our relaxed, hydrous glass densities at 298 K, 13.62 ± 0.24 cm³/mol, is in excellent agreement with the value of 13.21 ± 0.62 cm³/mol derived from the relaxed hydrous glasses at 298 K of Richet and Polian (*18*).

With an equation for the density of multicomponent silicate melts that includes H_2O, several geological problems can be addressed. There is a longstanding debate about the physical mechanisms by which tholeiitic basalts, the most prevalent magma type on Earth, differentiate as they solidify in the crust. Fractional crystallization has long been considered a primary mechanism for producing diverse igneous liquids. The details of this process, however, have been the focus of considerable controversy, and two opposing views have emerged. One theory holds that crystals grown near the roof and walls of a magmatic intrusion (where temperatures are lowest) are transported by gravitational forces to the floor of the chamber, much in the manner of clastic sediments in water (*19*). An alternative view argues that crystallization occurs primarily under in situ conditions along the base of the chamber (*20*).

One of the foremost objections to the concept of gravitational transport of crystals is based on the inference that plagioclase crystals found along the floor of many mafic layered intrusions are lighter than the postulated iron-rich liquids from which they crystallized (*21*). Tholeiitic liquids follow a trend of iron enrichment during differentiation, which typically peaks at FeO^T (total iron as FeO) values of ~15 weight % and more rarely at ~18 weight % (*22*). On the basis of melt density calculations and experimental measurements at 1 bar (*21*), it was shown that such iron-rich liquids are al-

Table 2. Experimental data. Density of the compressed glass at 298 K, $\rho^{glass}_{298\ K}$; relaxed liquid volume at $T_{f'}$ and 1 bar calculated from Eq. 1, $V^{meas}_{T_{f'}}$; and liquid volume at $T_{f'}$ and 1 bar calculated from Eq. 2, $V^{model}_{T_{f'}}$. OH is given as weight % H_2O; gfw, gram formula weight.

P (GPa)	T (K)	Time (hours)	Total H_2O (weight %)	$H_2O^{molecular}$ (weight %)	OH (weight %)	$\rho^{glass}_{298\ K}$ (g/cm³)	$T_{f'}$ (K)	α^{glass} (10^{-5}, K^{-1})	$V^{meas}_{T_{f'}}$ (cm³/gfw)	$V^{model}_{T_{f'}}$ (cm³/gfw)	Residual (%)
					KCS samples						
0.0	1400	12	0.00*	0.00	0.00	2.641	970	2.87	24.04	23.97	0.3
1.0	1400	43	0.20*	0.00	0.20	2.667	904	2.87	23.89	23.79	0.4
–	–	–	0.20*†	–	–	2.645	890	2.86	23.82	23.76	0.3
1.0	1500	49	0.21*	0.00	0.21	2.672	870	2.78	23.81	23.71	0.4
1.0	1500	20	0.65‡	0.00	0.65	2.668	758	2.63	23.50	23.36	0.6
0.9	1350	46	0.75	0.08	0.67	2.669	702	2.84	23.42	23.20	0.9
1.0	1400	48	2.38	0.77	1.61	2.627	640	2.79	22.85	22.71	0.6
1.0	1400	42	3.41‡	1.71	1.70	2.607	607	3.16	22.49	22.41	0.4
1.0	1400	22	4.75‡	2.93	1.83	2.572	555	3.45	22.11	21.99	0.5
1.0	1400	26	4.85‡	3.15	1.70	2.578	550	3.27	21.99	21.95	0.2
1.0	1400	25	5.64	3.55	2.09	2.548	530	3.36	21.86	21.73	0.6
1.0	1400	24	5.89	4.07	1.82	2.545	508	3.80	21.78	21.60	0.8
0.9	1245	47	6.14	3.96	2.18	2.521	519	3.55	21.86	21.59	1.2
					Rhyolitic samples						
0.0	1400	8	0.05*	0.00	0.05	2.324	1090	1.33	28.10	27.85	0.9
1.0	1400	31	0.19*	0.00	0.19	2.385	842	1.59	27.89	27.64	0.9
–	–	–	0.19*‡	–	–	2.325	955	1.42	27.90	27.74	0.6
1.0	1500	44	1.29	0.32	0.97	2.362	695	1.67	27.33	27.13	0.7
1.0	1500	25	1.91	1.05	0.85	2.327	590	1.94	27.29	26.79	1.8
1.0	1500	66	2.06	0.81	1.25	2.369	628	1.88	26.72	26.79	−0.3
1.0	1500	24	2.57	1.17	1.40	2.335	615	1.81	26.76	26.59	0.6
1.0	1500	46	4.71	3.02	1.69	2.297	531	2.38	25.86	25.72	0.5
1.0	1500	41	5.30	3.64	1.66	2.278	495	2.41	25.70	25.45	1.0
1.0	1500	22	5.92	4.36	1.56	2.269	448	2.78	25.43	25.14	1.1

*Samples not used in the regression †Sample is the previous sample after being heated and cooled through $T_{f'}$ three times and completely relaxed. ‡H_2O measured by manometry.

ways denser than the plagioclase on their liquidus, thus precluding crystal settling as the cause for the layering observed in mafic intrusions; and other mechanisms have been invoked [for example, oscillatory nucleation and subsolidus recrystallization (*23*)]. Before this work, the uncertainty in $\bar{V}_{H_2O}$ precluded a quantitative evaluation of the effect of dissolved water on the density of the iron-rich liquids, which can now be calculated.

Estimates of pre-eruptive water contents in tholeiitic basalts [up to 1 weight % H_2O (*24*)] are derived primarily from analyses on glasses from mid-ocean ridges and hot spots. Because H_2O is incompatible in the anhydrous phenocryst assemblage of tholeiitic basalts, crystallization causes both FeO^T and H_2O to increase in residual liquids. At a FeO^T concentration of 15.8 weight % [the peak value observed in an experimental tholeiitic liquid at the point of Fe-Ti oxide saturation (*25*)], only ~0.8 weight % dissolved water is required to render the liquid less dense than the coexisting plagioclase phenocrysts of An_{58} composition [2.699 g/cm^3 (*25*)]. Such a modest water content could arise after 40% crystallization of a tholeiitic basalt with an initial water content of 0.5 weight % H_2O.

The effect of water on the density of magmatic liquids also relates to models of convection within chambers, driven by thermal and compositional density gradients (*26*). The role of water in offsetting the effect of temperature to promote buoyant ascent of evolved melt along sidewall boundary layers was discussed by Shaw (*27*) and further explored by several others (*28*). The results of our study indicate that a gradient of only 0.16 and 0.25 weight % H_2O, respectively, is all that is required to offset the effect on melt density of a 100°C temperature gradient in a rhyolitic and basaltic melt at crustal depths.

References and Notes

1. M. C. Johnson, A. T. Anderson, M. J. Rutherford, *Rev. Mineral.* **30**, 281 (1994).
2. C. W. Burnham and N. F. Davis, *Am. J. Sci.* **270**, 54 (1971).
3. F. A. Ochs and R. A. Lange, *Contrib. Mineral. Petrol.* **129**, 155 (1997).
4. L. A. Silver *et al.*, *ibid.* **104**, 142 (1990).
5. B. O. Mysen, D. Virgo, F. A. Seifert, *Rev. Geophys. Space Phys.* **20**, 353 (1982).
6. R. A. Lange and I. S. E. Carmichael, *Geochim. Cosmochim. Acta* **51**, 2931 (1987).
7. ———, *Contrib. Mineral. Petrol.* **125**, 167 (1996).
8. G. Moore, T. Vennemann, I. S. E. Carmichael, *Am. Mineral.* **83**, 36 (1998).
9. C. T. Moynihan, *Rev. Mineral.* **32**, 1 (1995); J. A. Tangeman, thesis, University of Michigan, Ann Arbor, MI (1998). The value of T_f' is approximated (±20°C) by the onset of the rapid rise in a glass thermal expansion curve during heating.
10. The density is converted to molar volume as follows: $V^{glass}_{298\ K}$ = gram formula weight/$\rho^{glass}_{298\ K}$
11. Y. Zhang *et al.*, *Geochim. Cosmochim. Acta* **61**, 3089 (1997) was used for calibration of the FTIR measurements of water (±0.7% relative) on rhyolite glasses. The manometry technique of T. W. Vennemann and J. R. O'Neil [*Chem. Geol.* **103**, 227 (1993)] was used to measure water contents in four KCS glasses (H_2O collection ≥150°C); these data (±0.5% relative) were used to calibrate the FTIR measurements on the remaining KCS glasses. The fitted molar absorptivities for the 5300 cm^{-1} ($H_2O^{molecular}$) and the 4540 cm^{-1} (OH) FTIR bands are 5.90 ± 1.19 cm^2/mol and 4.48 ± 1.04 cm^2/mol, respectively. These errors translate to uncertainties of <0.2 weight % H_2O (absolute).
12. A pressure correction per gigapascal of 2.52 (±0.25) % for the rhyolitic glasses and 1.06 (±0.25) % for the KCS glasses was obtained by comparing the difference between the 1-bar and 1-GPa densities of several anhydrous glasses of each composition. Consistent with a similar correction for hydrous albitic glasses (*3*), there is no evidence that the pressure corrections vary with H_2O concentration, within experimental resolution.
13. R. A. Lange, *Geochim. Cosmochim. Acta* **60**, 4989 (1996); *Contrib. Mineral. Petrol.* **130**, 1 (1997).
14. J. Bockris, J. W. Tomlinson, J. L. White, *Faraday Soc. Trans.* **52**, 299 (1956); D. J. Stein, J. F. Stebbins, I. S. E. Carmichael, *J. Am. Ceram. Soc.* **69**, 396 (1986).
15. M. L. Rivers and I. S. E. Carmichael, *J. Geophys. Res.* **92**, 9247 (1987); V. C. Kress, Q. Williams, I. S. E. Carmichael, *Geochim. Cosmochim. Acta* **52**, 288 (1988); V. C. Kress and I. S. E. Carmichael, *Contrib. Mineral. Petrol.* **108**, 82 (1991).
16. The calculations were done with the compilation in (*7*) and that in R. A. Lange and I. S. E. Carmichael, *Rev. Mineral.* **24**, 25 (1990).
17. Propagated uncertainties in $V^{liq}_{T_f'}$ are ~1.1%, with the largest contributions to the error arising from the following three terms: (i) the Archimedean measurement of $\rho^{glass}_{298\ K}$ (<0.2%), (ii) the pressure correction to density (~0.25%), and (iii) the error in the gram formula weight (~0.4%) that is primarily derived from the analytical uncertainty in measuring the H_2O concentration. The uncertainty in α^{glass} of ±15% and in $T_{f'}$ of ±20°C each contribute <0.1% error to values of $V^{liq}_{T_f}$.
18. P. Richet and A. Polian, *Science* **281**, 396 (1998).
19. L. R. Wager and G. M. Brown, *Layered Igneous Rocks* (Oliver & Boyd, Edinburgh, 1968); T. N. Irvine, J. C. O. Andersen, C. K. Brooks, *Geol. Soc. Am. Bull.* **110**, 1398 (1998).
20. I. H. Campbell, *Lithos* **11**, 311 (1978); A. R. McBirney and R. M. Noyes, *J. Petrol.* **20**, 487 (1979).
21. Y. Bottinga and D. Weill, *Am. J. Sci.* **269**, 169 (1970); I. H. Campbell, P. L. Roeder, J. M. Dixon, *Contrib. Mineral. Petrol.* **67**, 369 (1978).
22. D. J. Fornari *et al.*, *J. Geophys. Res.* **88**, 10519 (1983).
23. G. Brandeis and C. Jaupart, in *Origin of Igneous Layering*, I. Parsons, Ed. (Reidel, Boston, 1987), pp. 613–639; A. E. Boudreau and A. R. McBirney, *J. Petrol.* **38**, 1003 (1997).
24. D. W. Muenow *et al.*, *Nature* **343**, 159 (1990); P. J. Wallace and A. T. Anderson, *Bull. Volcanol.* **59**, 327 (1998).
25. D. Snyder, I. S. E. Carmichael, R. A. Wiebe, *Contrib. Mineral. Petrol.* **113**, 73 (1993).
26. R. J. S. Sparks, H. E. Huppert, J. S. Turner, *Philos. Trans. A R. Soc. London* **310**, 511 (1984); J. S. Turner and I. H. Campbell, *Earth Sci. Rev.* **23**, 255 (1986); D. Martin, R. W. Griffiths, I. H. Campbell, *Contrib. Mineral. Petrol.* **96**, 465 (1987).
27. H. R. Shaw, *Carnegie Inst. Wash. Publ.* **634**, 139 (1974).
28. F. Spera, D. A. Yuen, D. V. Kemp, *Nature* **310**, 764 (1984); A. R. McBirney, B. H. Baker, R. H. Nilson, *J. Volcan. Geotherm. Res.* **24**, 1 (1985); A. Trial and F. Spera, *Geol. Soc. Am. Bull.* **102**, 353 (1990).

29. Supported by NSF (grant EAR-9706075). We thank I. Carmichael, E. Essene, D. Snyder, F. Spera, and two anonymous reviewers for their insightful comments.

16 October 1998; accepted 7 December 1998

Convergence of Transforming Growth Factor–β and Vitamin D Signaling Pathways on SMAD Transcriptional Coactivators

Junn Yanagisawa,[1] Yasuo Yanagi,[1] Yoshikazu Masuhiro,[1] Miyuki Suzawa,[1,2] Michiko Watanabe,[1] Kouji Kashiwagi,[1] Takeshi Toriyabe,[1] Masahiro Kawabata,[3] Kohei Miyazono,[3] Shigeaki Kato[1,2]*

Cell proliferation and differentiation are regulated by growth regulatory factors such as transforming growth factor–β (TGF-β) and the liphophilic hormone vitamin D. TGF-β causes activation of SMAD proteins acting as coactivators or transcription factors in the nucleus. Vitamin D controls transcription of target genes through the vitamin D receptor (VDR). Smad3, one of the SMAD proteins downstream in the TGF-β signaling pathway, was found in mammalian cells to act as a coactivator specific for ligand-induced transactivation of VDR by forming a complex with a member of the steroid receptor coactivator–1 protein family in the nucleus. Thus, Smad3 may mediate cross-talk between vitamin D and TGF-β signaling pathways.

Vitamin D receptor (VDR) is a member of the nuclear receptor superfamily, and acts as a ligand-inducible transcriptional factor with coactivators (*1, 2*) such as the members of the steroid receptor coactivator–1/transcriptional intermediary factor 2 (SRC-1/TIF2) proteinfamily (*3*) and CREB-binding protein (CBP)/p300 (*4*). Cooperative actions of the growth regulatory factor TGF-β and vitamin D (*5*), and the phenotype of VDR knock-out mice (*6*), indicate that there may be cross-talk between the two signaling pathways. We therefore examined ligand-induced transactivation function of VDR and other nuclear receptors in cells stimulated by TGF-β or bone morphogenetic protein (BMP). VDR expression vectors and

The Density of Hydrous Magmatic Liquids

Frederick A. Ochs III and Rebecca A. Lange (February 26, 1999)

Science **283** (5406), 1314-1317. [doi: 10.1126/science.283.5406.1314]